Journal of Applied Polymer Science

Nonisothermal crystallization and morphology of crystallites of polyamide 66 and copolyamide 66 containing 2-carboxyethyl phenyl phosphinic acid

Sheng Long Tan,[1,2] Lian Xin Ma,[1] Xiao Guang Sun,[1] Xu Dong Tang[1]

[1]School of Materials Science and Chemical Engineering, Tianjin University of Science and Technology, Tianjin 300457, China

[2]College of Life Science and Technology, Huazhong University of Science and Technology, Wuhan 430074, China

Correspondence to: X.D. Tang (E-mail: tangxd@tust.edu.cn)

ABSTRACT: Flame-retardant polyamide 66 with a 10% mass fraction of 2-carboxyethyl phenyl phosphinic acid (CEPPA) hexamethylene diamine salt (PA66-10) was fabricated in our previous study. In this study, the nonisothermal crystallization kinetics of pure polyamide 66 (PA66-0) and PA66-10 were measured by differential scanning calorimetry, and the data obtained were analyzed, and we calculated the average Avrami exponent (n) and used the Jeziorny, Mo, and Kissinger methods. The results from all of these methods show that the crystallization mechanism of PA66-0 mainly consisted of three stages, whereas PA66-10 mainly consisted of two stages. At the prime stage, both PA66-0 and PA66-10 may have had the same crystallization mechanism. When the cooling rates were 15 and 20°C/min, the approximate n suggested that the growth form of the spherulite mode in PA66-0 may have been complicated, whereas PA66-10 may have had a one-dimensional, two-dimensional space-extension, circular, diffusion controlled growth. The crystallization activation energies were determined to be 183.2 and 301 kJ/mol for PA66-0 and PA66-10, respectively, by the Kissinger method. To further study the influence of the addition of CEPPA on the crystallization behaviors of PA66-0, the spherulitic morphologies were examined by polarized light microscopy. © 2014 Wiley Periodicals, Inc. J. Appl. Polym. Sci. **2015**, *132*, 41790.

KEYWORDS: crystallization; flame retardance; kinetics

Received 16 December 2013; accepted 22 November 2014
DOI: 10.1002/app.41790

INTRODUCTION

The most prominent feature of polyamide 66 is its excellent wearability. Therefore, polyamide 66 fibers are widely used in the making of military and civilian clothing. However, the flame retardancy of polyamide 66 is not good, and it is viewed as a combustible material according to the standard of the limiting oxygen index. So, research on flame-retardant polyamide 66 has great significance. As a bifunctional reactive flame retardant, 2-carboxyethyl phenyl phosphinic acid (CEPPA) has been widely used in the flame-retardant field for polymer modification, especially in poly(ethylene terephthalate).[1–3] Until now, few people have studied flame-retardant polyamide 66 through the addition of CEPPA. One patent literature[4] reported the copolymerization of CEPPA and nylon 66 salt with only a 2.38% mass fraction of CEPPA hexamethylene diamine salt, and it showed that the copolymer had a good flame retardancy without an obvious reduction in the mechanical properties. However, the influence of the addition of CEPPA on the crystallization properties of pure polyamide 66 (PA66-0) has not been studied.

In our previous study,[5] the flame-retardant polyamide 66 containing CEPPA (PA66-10) was fabricated, and its chemical structure, flame-retardant performance, and thermal stability were also studied. In virtually every melt process, the polymer melt is subjected to shearing and nonisothermal crystallization conditions. Therefore, it is of practical importance and necessity to study the nonisothermal crystallization kinetics. In this study, we mainly focused on the influence of the addition of CEPPA on the crystallization properties of PA66-0 by differential scanning calorimetry (DSC). The crystallization kinetics parameters and mechanism containing the average Avrami exponent (n), the crystallization activation energy (ΔE) were obtained with the Jeziorny, Mo, and Kissinger methods. In addition, polarized light microscopy (PLM) is one of the predominant and most informative tools used for investigating spherulitic morphologies. So, the spherulitic morphologies of both PA66-0 and PA66-10 were studied under different isothermal crystallization times (ts) to further study the influence of the addition of CEPPA on the crystallization behaviors of PA66-0.

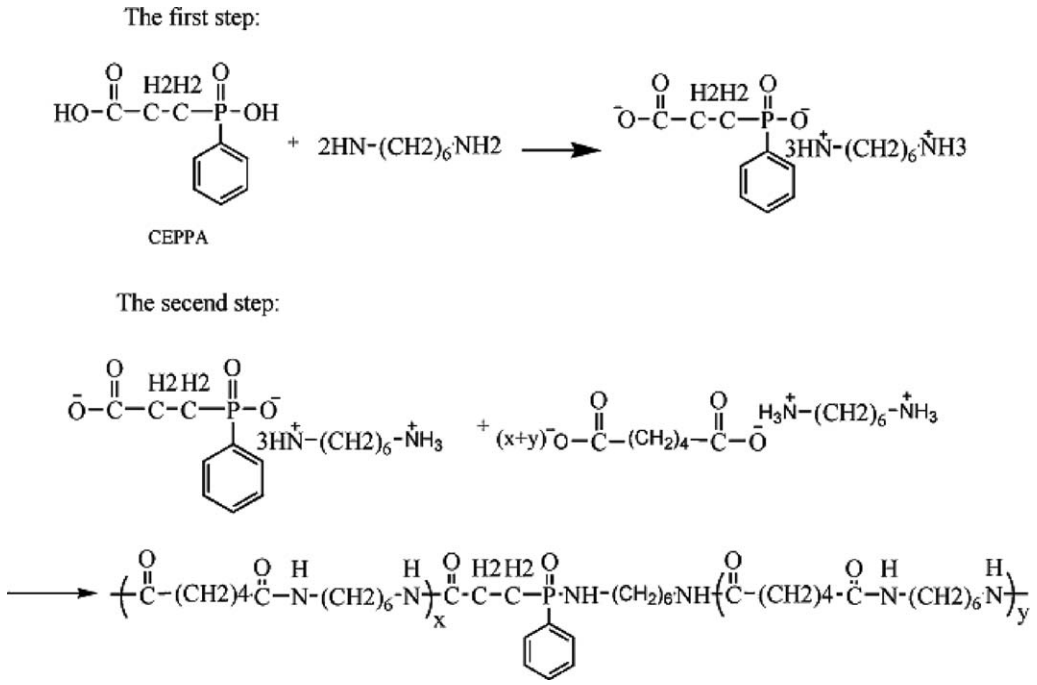

Figure 1. Fabrication process for PA66-10.

EXPERIMENTAL

Materials

The CEPPA used in this study was synthesized in our laboratory according to our earlier study.[6] 1,6-Diaminohexane and adipic acid were both purchased from Sinopharm Chemical Reagent Co., Ltd. (Beijing, China). Nylon 66 salt was purchased from Anshan Guorui Chemical Co., Ltd. (Liaoning Province, China).

Fabrication Process for PA66-10

PA66-10 was fabricated according to a method given in the literature.[4] To compare the difference in the thermolysis kinetics between PA66-10 and PA66-0, PA66-0 was also fabricated with the same method. The fabricating process of PA66-10 is shown in Figure 1.

Nonisothermal Crystallization Kinetics Testing for PA66-0 and PA66-10

The DSC processes of PA66-0 and PA66-10 were conducted with a NETZSCH5 DSC analyzer (Netzsch, Shanghai, China). The all samples were dried at 80°C *in vacuo* for 12 h before measurement. During the testing process, all of the samples were first heated from room temperature to 300°C at a heating rate of 10 K/min under a nitrogen purge with a flow rate of 40 mL/min. We retained this temperature for 3 min and cooled the sample to room temperature at cooling rates (Φ) of 5, 10, 15, and 20 K/min. The data were analyzed and processed with Proteus analysis software and Origin7.5 software.

Data Processing Methods

The isothermal crystallization kinetics analysis of the polymeric materials were based on the Avrami equation:[7]

$$X_t = 1 - \exp(-Z_t^n) \tag{1}$$

where X_t is the crystallinity at a certain crystallization time and temperature, or the relative crystallinity; Z is the crystallization rate constant; and t is the crystallization time.

Jeziorny Method

According to the literature,[8,9] the Jeziorny equation can be obtained with a series of mathematical methods:

$$\log[-\ln(1-X_t)] = n\log t + \log Z \tag{2}$$

When the value of Φ is fixed, Z at a certain Φ could be obtained by the slope and interception value of $\log[-\ln(1-X_t)]$ versus $\log t$, respectively. Because of the effect of different Φ, Jeziorny[10] suggested that Z should be corrected though eq. (3):

$$\ln Z_c = \ln Z/\Phi \tag{3}$$

where Z_c is the modified crystallization rate constant.

Mo Method

After the Avrami equation [eq. (1)] and the Ozawa equation [eq. (4)] were combined, Mo's equation [eq. (5)][11] can be obtained, and it has been successfully used in nylon 1212[12] and nylon 11:[13]

$$\log[-\ln(1-X_t)] = \log P(T) - m\log\ \Phi \tag{4}$$

$$\log\ \Phi = \log F(T) - a\log t \tag{5}$$

where $P(T)$ is the cooling function, m is the Ozawa index, a is m/n, and $F(T) = [P(T)/Z]^{1/m}$, which is correlated with the crystallization rate, and its physical meaning is that a Φ needs to be chosen to achieve a certain degree of crystallization per unit time.[14] When the value of X_t is fixed, the values of a and $F(T)$ can be obtained by the slope and intercept value of $\log \Phi$ versus $\log t$.

Kissinger Method

According to the literature,[15,16] ΔE can be obtained from the Kissinger equation:

$$d\left[\ln\left(\Phi/T_p^2\right)\right]/d\left(1/T_p\right) = -\Delta E/R \tag{6}$$

where T_p is the temperature at peak (K) and R is the universal gas constant [J (K mol)$^{-1}$]. During the cooling process, $1/T_p$ is

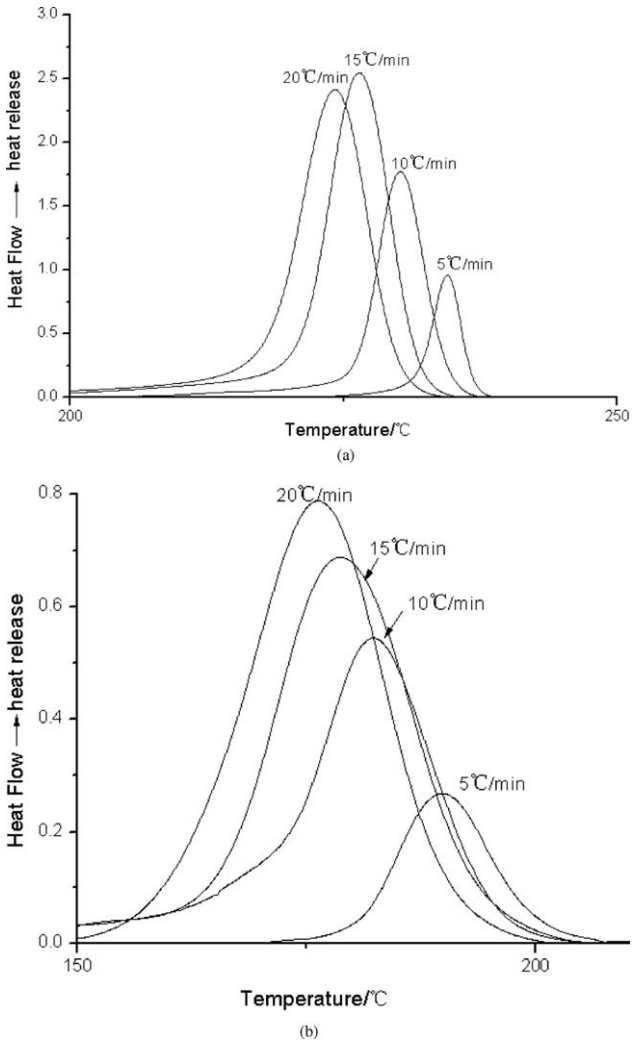

Figure 2. DSC curves of (a) PA66-0 and (b) PA66-10 at different Φs.

always replaced by $-1/T_p$. In our study, when Φ was fixed, different $\ln(\Phi/T_p^2)$ and $-1/T_p$ values were obtained. Then, ΔE was obtained by the slope value of $\ln(\Phi/T_p^2)$ versus $-1/T_p$.

Polarizing Optical Microscopy (POM) Tests

The polymer sample, sandwiched between two glass slides, was first melted for 5 min. After it was pressed with a weight of 500 g, the sample was quickly transferred to an oil bath (dimethyl silicone), which was preheated to 220°C for the isothermal crystallization study. The spherulitic morphologies were then examined with PLM (Olympus SZX7).

RESULTS AND DISCUSSION

DSC Analysis

The DSC curves of PA66-0 and PA66-10 in a nitrogen atmosphere at different Φs are shown in Figure 2(a,b); it shows that the crystallization exothermic peak shifted obviously to a lower temperature range when CEPPA was incorporated into PA66-0. This indicated that there was more time for PA66-10 to pack into the crystal lattice at the same Φ compared with PA66-0. As shown in Figure 3, at a given Φ, the crystallization exothermic peak gradually shifted to lower temperature ranges with the

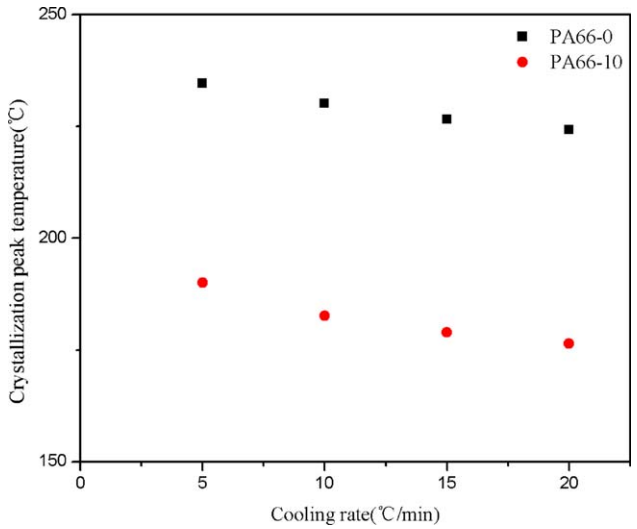

Figure 3. Plots of T of the crystallization exothermic peak at different Φs. [Color figure can be viewed in the online issue, which is available at wileyonlinelibrary.com.]

introduction of CEPPA into PA66-0; this meant that the nonisothermal crystallization capacity of the samples decreased gradually. The crystallization enthalpy (ΔH_c) of the samples were also recorded (Table I). The ΔH_c value increased with increasing Φ from 5 to 15°C/min but decreased then. It seemed that an appropriate Φ existed to form more perfect crystals and reach a higher degree of crystallinity. When Φ was 15°C/min, the largest ΔH_c was obtained. Although PA66-10 formed a perfect crystal in the range 10–15°C/min. In addition, the incorporation of CEPPA into PA66-0 decreased the ΔH_c value; this meant that CEPPA may have had a negative influence on the crystallization of PA66-0.

Average Avrami Parameter

A new method was first reported[17] to determine n (The Average Avrami Parameter) from experimental crystallization exotherms with a peak temperature where the crystallization rate is maximum (T^*) and two inflexion points (T_1 and T_2) for different Φ. This method has been successfully used to calculate n of nylon 1212.[18] So, we tried to calculate the n values of PA66-0 and PA66-10 with this method.

The plots of X_t versus temperature (T) for PA66-0 and PA66-10 are shown in Figure 4(a,b), respectively.

Table I. Values of T_p, T_0 (the crystallization onset temperature), $t_{1/2}$ (the half-time of crystallization), and ΔH_c for PA66-0 and PA66-10

Sample	Φ (°C/min)	T_p (°C)	T_0 (°C)	$t_{1/2}$ (min)	ΔH_c (J/g)
PA66-0	5	234.6	237.6	0.64486	51.9
	10	230.2	234.5	0.43371	67.8
	15	226.5	231.7	0.35923	78.8
	20	224.3	229.8	0.29028	62.8
PA66-10	5	190.1	200.3	2.05326	43.8
	10	182.7	195.2	1.26325	53.5
	15	179	193.5	0.9584	54.3
	20	176.5	190.5	0.73289	47.1

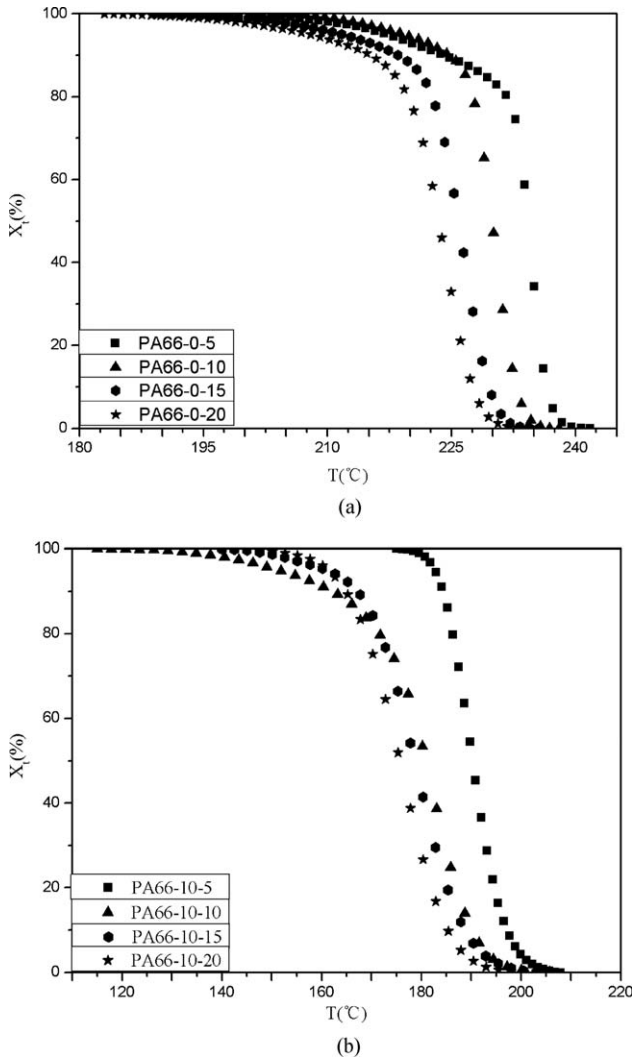

Figure 4. Plots of X_t versus T for (a) PA66-0 and (b) PA66-10.

To identify the exact values of T^*, T_1, and T_2, the first-order and second-order differentials of the plots of X_t versus T were calculated by origin software. Then, we obtained the plot of T versus ln Φ for PA66-0 and PA66-10; these are shown in Figures 5(d) and 6(d).

According to theory, these temperatures, including T^*, T_1, and T_2, varied linearly with the Φ logarithm.[19] However, it was obvious that the three lines were not parallel to each other. We supposed that the lines may have diverged at certain Φ, and the lines under only two Φ were studied. The results are shown in Figures 5 and 6.

These plots showed that when Φ were 15 and 20°C/min; the three lines in PA66-0 and PA66-10 seemed parallel to each other. At lower that this Φ value (<15°C/min), the values of T_1, T^*, and T_2 decreased considerably when ln Φ increased. To identify the depth of parallelism, we calculated the distance between T_1 and T^* and T_1 and T_2. The results are listed in Table II.

Table II shows that the three lines were not absolutely parallel with each other, and the depth of parallelism of PA66-10 was lower than that of PA66-0. With these deviations, we calculated n approximately and compared the difference between PA66-0 and PA66-10 in crystallization kinetics. Therefore, in a general manner, T_1, T^*, and T_2 may be expressed as $T_i = A \ln \Phi + B_i$ (T_1 is the first inflexion point; T_2 is the second inflexion point; A = n/a(a from the equation: ln $K(T)$ = aT + b), $K(T)$ is cooling function); $B_1 = ([(\mathrm{In}(3-\sqrt{5})/2]-\mathrm{b})/\mathrm{a})$; $B_2 = ([(\mathrm{In}(3+\sqrt{5})/2]-\mathrm{b})/\mathrm{a}))$ according to the literature.[18] The n values of PA66-0 and PA66-10 were obtained as 8.89 and 1.83, respectively; this showed that the growth form of the spherulite mode in PA66-0 may have been complicated[20] because of the spherulites' impingement and crowding. However, PA66-10 may have had a one-dimensional, two-dimensional space-extension, circular, diffusion-controlled growth at these Φ.

Nonisothermal Crystallization Kinetics

To analyze the nonisothermal crystallization kinetics data, X_t was calculated. The plots of X_t versus time for PA66-0 and PA66-10 are shown in Figure 7(a,b), respectively. We observed that more time was needed for the sample to reach the same X_t with decreasing Φ. In fact, the crystallization started at higher temperatures, and the crystallization rate of the sample was slower than the lower temperature because of the lower supercooling. It was interesting that PA66-10 needed more time to reach the same crystallization at the same Φ compared to PA66-0; this also indicated that CEPPA in PA66-10 restricted the crystallization of PA66-0 just as it influenced ΔH_c. Two widely used methods, Jeziorny's and Mo's methods, were used to analyze the nonisothermal crystallization kinetics of PA66-0 and PA66-10.

Calculation of the Crystallization Kinetics Parameters with the Jeziorny Method

The nonisothermal crystallization could be described by the Avrami equation on the basis of the assumption that the crystallization temperature was constant. The plots of log t versus log[$-\ln(1 - X_t)$] for PA66-0 and PA66-10 are shown in Figure 8. The correlation coefficient (R; from this point on), n, Z, and Z_c were obtained and are listed in Table III. The high linear Rs for PA66-0 and PA66-10 suggested that this method was effective. According to the literature,[8] n was related to the mechanism and growth modes of nucleation, whereas n in noncrystallization kinetics did not have definite physical meaning, but some useful information could also be obtained from the average of n at different Φ.[21] The average ns for PA66-0 and PA66-10 were 1.184 and 1.084, respectively; this suggested that PA66-10 may have had a crystallization mechanism similar to that of PA66-0 at the prime stage. The Z_c related to temperature included two aspects: nucleation and crystallization. The higher the value of Z_c was, the faster the rate of crystallization was. From the Z_c value listed in Table III, we observed that PA66-0 had a slightly lower Z_c value at a given Φ; this indicated that the incorporation of CEPPA may have retarded the crystallization of the PA66-0 at the primary stage.

To further confirm the difference in the crystallization mechanisms[18] between PA66-0 and PA66-10, we plotted the first-order differential of log t versus log[$-\ln(1 - X_t)$] [Figure 9(a,b)]

The shape of the curves from these two figures showed that the crystallization mechanism of PA66-0 mainly contained three parts: the linear part with slopes equal to 1 at the prime stage; the saddle-shaped part, with slopes of greater than 1 and which showed great changes with increasing log t, and the third part,

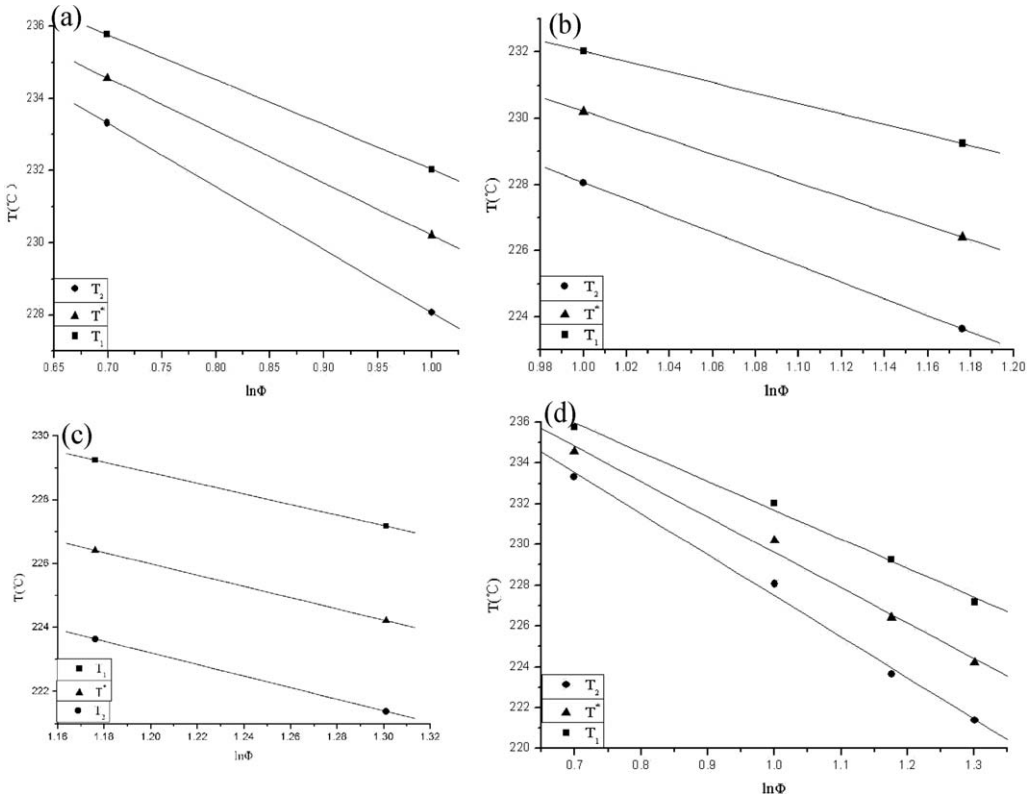

Figure 5. Plots of T versus ln Φ for PA66-0: (a) Φ = 5 and 10°C/min, (b) Φ = 10 and 15°C/min, (c) Φ = 15 and 20°C/min, and (d) Φ = 5, 10, 15, and 20/min.

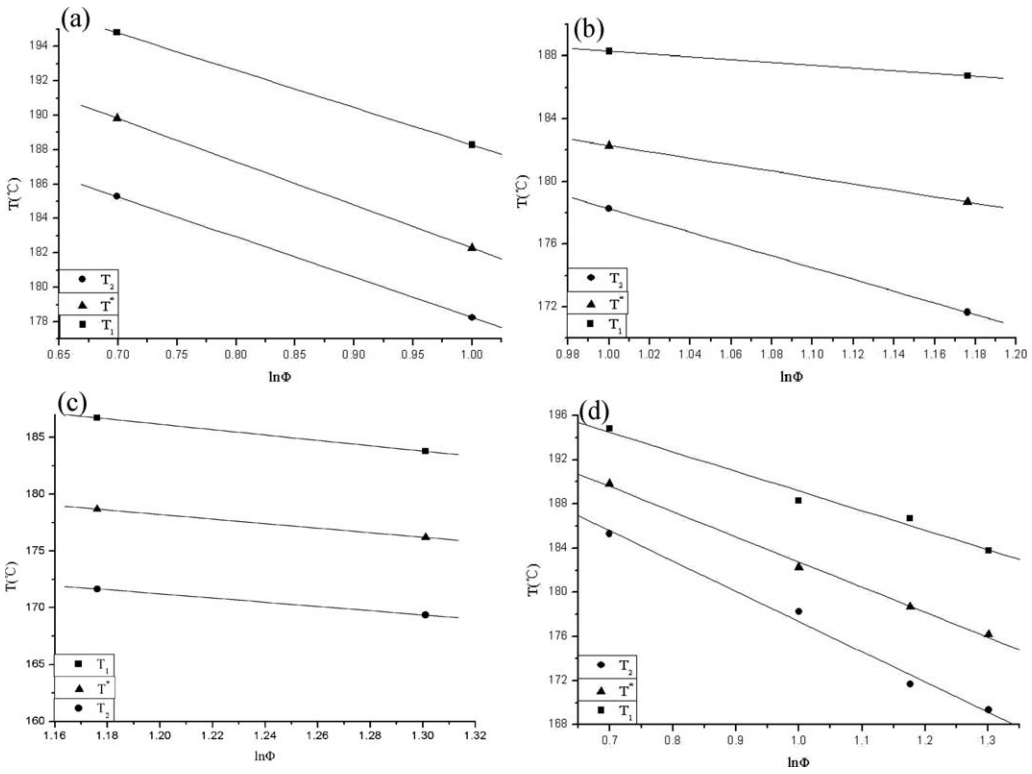

Figure 6. Plots of T versus ln Φ for PA66-10: (a) Φ = 5 and 10°C/min, (b) Φ = 10 and 15°C/min, (c) Φ = 15 and 20°C/min, and (d) Φ = 5, 10, 15, and 20°C/min.

Table II. Values of T_1, T^*, and T_2 and Relative Deviations of $T^* - T_2$ to $T_1 - T^*$ for PA66-0 and PA66-10

	Φ (°C/min)	T_1 (°C)	$T_1 - T^*$ (°C)	T^* (°C)	$T^* - T_2$ (°C)	T_2 (°C)	Relative deviation of $(T^* - T_2)$ to $(T_1 - T^*)$ (%)
PA66-0	15	229.24	2.83	226.41	2.77	223.64	2.12
	20	227.17	2.96	224.21	2.83	221.38	4.39
PA66-10	15	186.71	8.02	178.69	7.04	171.65	12.22
	20	183.76	7.57	176.19	6.85	169.34	9.51

with slopes of less than 1 and which had a small changes, with increasing log *t*. Although the crystallization mechanism of PA66-10 mainly contained two parts: the linear part with slopes equal to 1 at the prime stage and the saddle-shaped part with slopes greater than 1. The slopes equal to 1 that remained constant indicated that the plots of $\log[-\ln(1 - X_t)]$ versus log *t* showed a line, greater or less than 1 with changed slopes and showed a nonline. This confirmed that the Jeziorny method was just reasonable at the prime stage of crystallization. In addition, these figures suggest that the crystallization mechanism of PA66-0 was more complicated than PA66-10; this was concordant with the results of the analysis of *n* of PA66-0 and PA66-10 discussed previously.

Calculation of the Crystallization Kinetics Parameters with Mo's Method

The plots of log Φ versus log *t* for PA66-0 and PA66-10 are shown in Figure 10. We observed that a good linear relationship for PA66-0 and PA66-10 was obtained; this indicated that Mo's method could be used reasonably. *R*, *n*, and $F(T)$ were obtained and are listed in Table IV. The value of $F(T)$ increased with increasing crystallinity; this indicated that the crystallization rate decreased with increasing crystallinity. The values of $F(T)$ in PA66-10 were higher than that in PA66-0; this suggested that the crystallization rate of PA66-10 was lower than that of PA66-0 during the nonisothermal crystallization process.

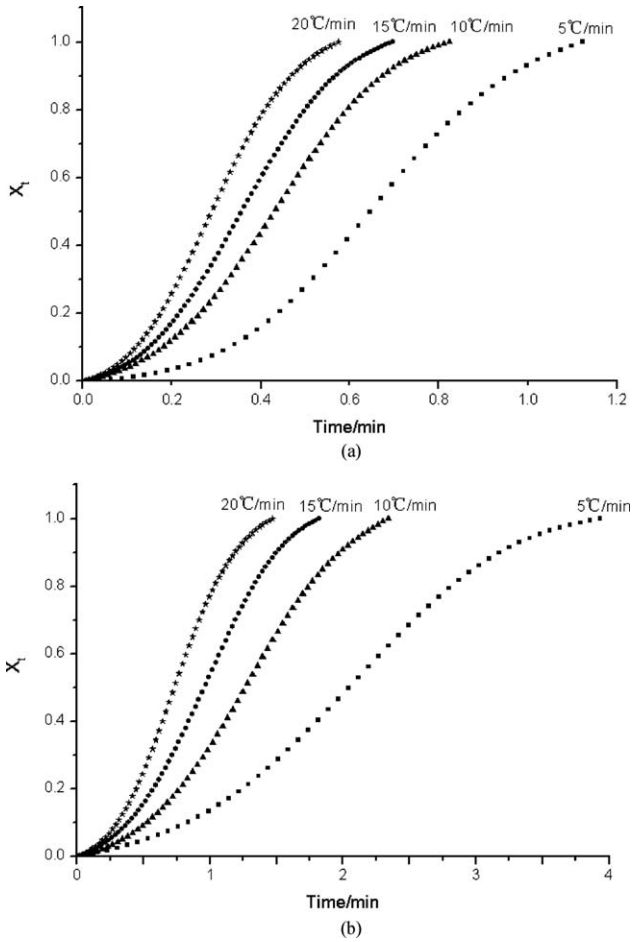

Figure 7. X_t and *T* at different *t*s during the process of nonisothermal crystallization for (a) PA66-0 and (b) PA66-10.

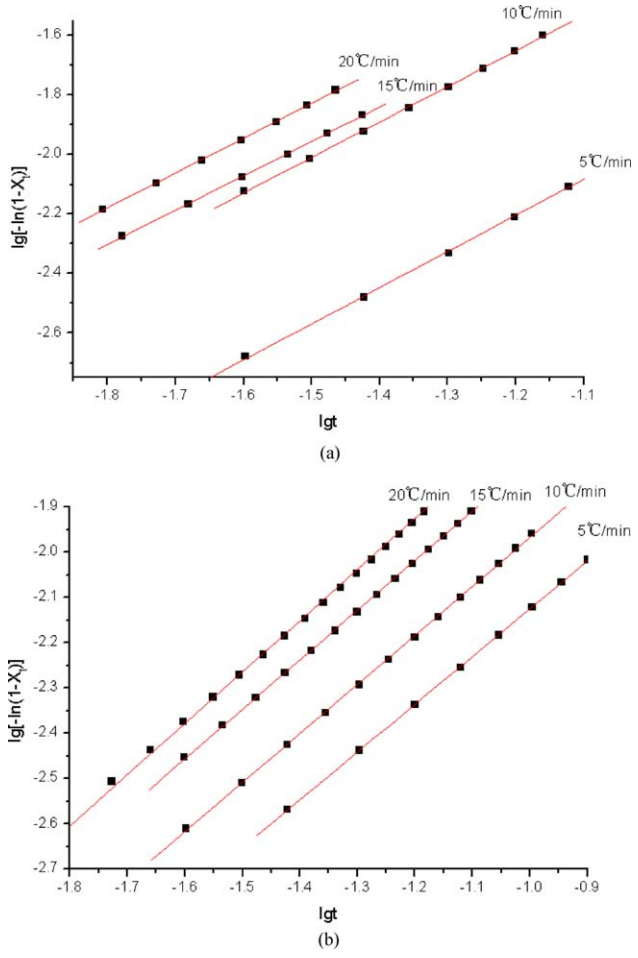

Figure 8. Plots of log *t* versus $\log[-\ln(1 - X_t)]$ for (a) PA66-0 and (b) PA66-10. [Color figure can be viewed in the online issue, which is available at wileyonlinelibrary.com.]

Table III. Values of R, n, Z, and Z_c for PA66-0 and PA66-10 by the Jeziorny Method

	Φ (°C/min)	R	n	Z	Z_c
PA66-0	5	0.99908	1.21549	0.179	0.70888
	10	0.99943	1.19385	0.6	0.9502
	15	0.99974	1.15524	0.6	0.96652
	20	0.99973	1.17172	0.85	0.99191
PA66-10	5	0.99994	1.05447	0.085	0.61078
	10	0.99978	1.05447	0.13	0.81544
	15	0.99971	1.09681	0.2	0.89826
	20	0.99929	1.13245	0.27	0.93663

Calculation of the ΔE with the Kissinger Method

The plots of $\ln(\Phi/T_p^2)$ versus $1/T_p$ for PA66-0 and PA66-10 are shown in Figure 11, and the ΔE and R values are listed in Table V. Good R values for PA66-0 and PA66-10 indicated that both the experimental data and the results were reliable. The obtained ΔE values of PA66-0 and PA66-10 were 183.2 and 301 kJ/mol(Table V), respectively. The larger value of ΔE for PA66-10 indicated that more energy was needed for PA66-10 to crystallize than for PA66-0; this indicated that PA66-10 was harder to crystallize than PA66-0.[22] This result was also concordant with those of both Jeziorny's and Mo's methods.

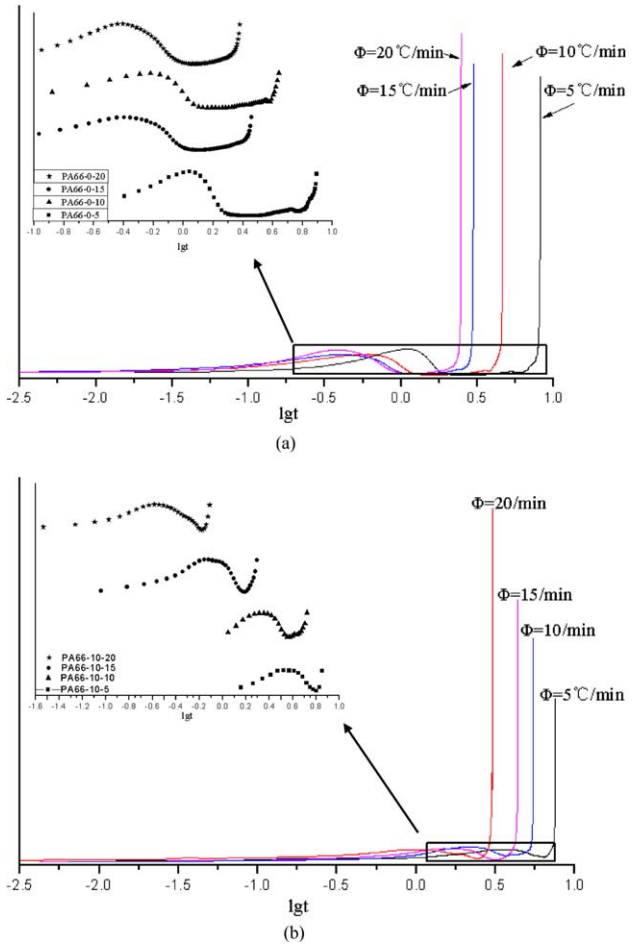

Figure 9. First-order differential of log t versus $\log[-\ln(1-X_t)]$ for (a) PA66-0 and (b) PA66-10. [Color figure can be viewed in the online issue, which is available at wileyonlinelibrary.com.]

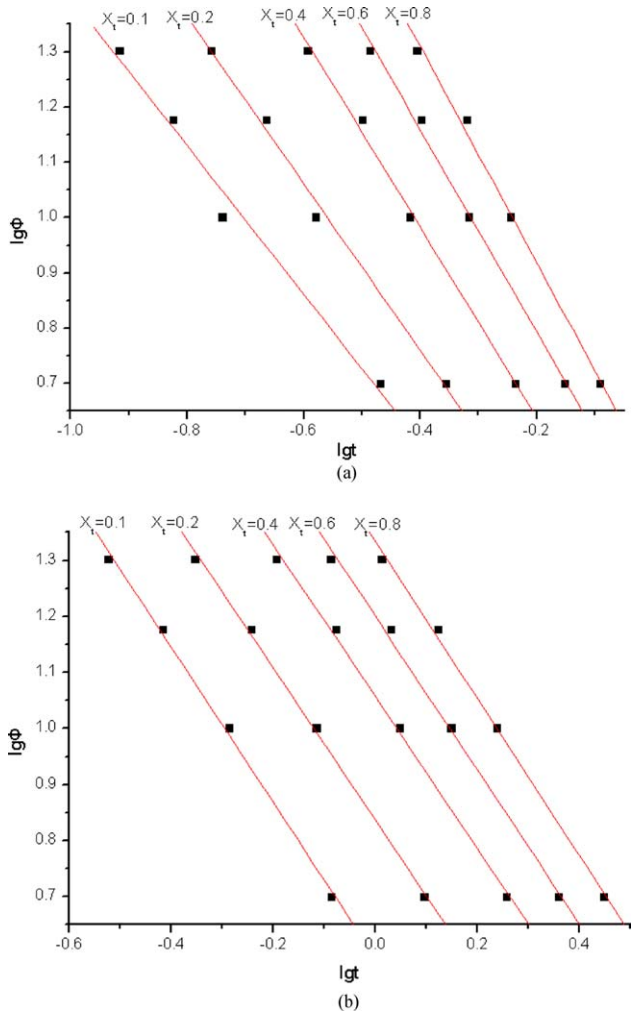

Figure 10. Plots of log t versus log Φ curve for (a) PA66-0 and (b) PA66-10. [Color figure can be viewed in the online issue, which is available at wileyonlinelibrary.com.]

Table IV. Values of X_t, R, n, and $F(T)$ for PA66-0 and PA66-10 by Mo's Method

	X_t	R	$F(T)$	a
PA66-0	0.1	0.98497	1.14	1.34098
	0.2	0.99384	1.43	1.50789
	0.4	0.99589	1.97	1.71986
	0.6	0.99661	2.67	1.83097
	0.8	0.99499	3.78	1.90448
PA66-10	0.1	0.99732	3.9	1.38348
	0.2	0.99804	6.88	1.35048
	0.4	0.99647	11.4	1.3516
	0.6	0.99636	15.8	1.36857
	0.8	0.99779	21.6	1.39824

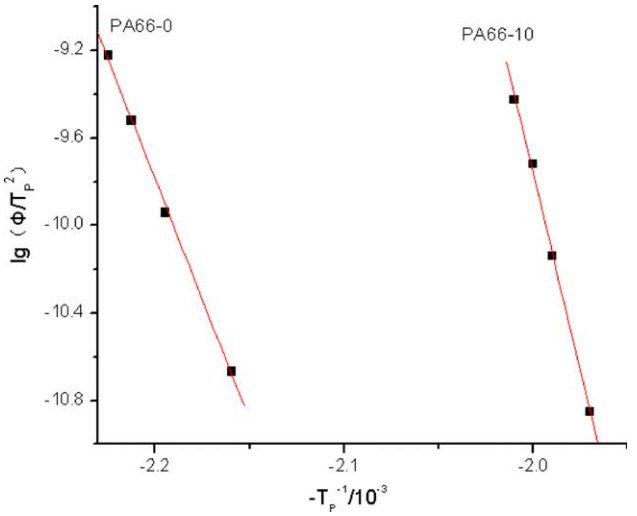

Figure 11. Plots of $\ln(\Phi/T_p^2)$ versus $1/T_p$ for PA66-0 and PA66-10. [Color figure can be viewed in the online issue, which is available at wileyonlinelibrary.com.]

Crystallite Morphology

In fact, there were many factors that influenced the spherulitic morphology, including the isothermal *t*, crystallization temperature, Φ, and stress. To study the influence of the addition of CEPPA to PA66 on the spherulitic morphology of PA66, the isothermal *t* was regarded as the only changed condition; meanwhile, we kept the isothermal crystallization temperature at 220°C. We kept the stress the same by pressing the sample with a weight of 500 g, and we retained the same Φ by transferring the sample under a isothermal *t* to an ice–water bath.

PLM is one of the predominant and most informative tools used for investigating spherulitic morphologies. Figure 12 shows a series of PLM micrographs of PA66-0 and PA66-10 spherulites formed at different isothermal *t* values. The Maltese cross extinction patterns along the vibrational directions of the polarizer and the analyzer are shown clearly in Figure 12. All of the spherulites exhibited colorful birefringence under the crossed polars. The sign of the birefringence was determined with a primary red filter (λ plate) located diagonally between the crossed polars. When the spherulite was negative, its first and third quadrants were yellow, and the second and fourth ones were blue. For a positive spherulite, the first and third quadrants were blue, and the second and fourth ones were yellow. If the color differences between the four quadrants could not be clearly discerned, the spherulite was a mixed one. The morphologies of the PA66 and PA66-10 spherulites and the sign of their birefringence were found to depend on the isothermal *t* and T_c (Table V). During the isothermal *t*s from 2.5 to 30 min, the spherulites were sparsely distributed and appeared with

Table V. ΔE and *R* Values for PA66-0 and PA66-10

	R	ΔE (kJ/mol)
PA66-0	0.99851	183.2
PA66-10	0.99775	301

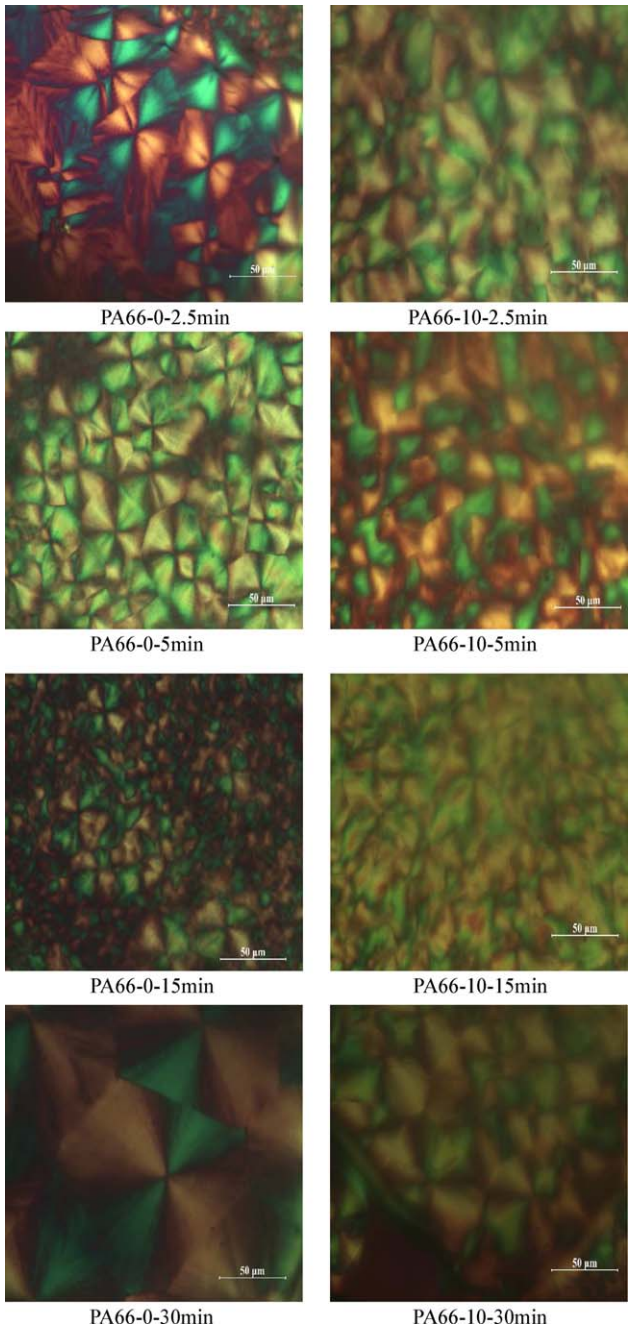

Figure 12. Micrographs of the PA66 and PA66-10 spherulites formed at different isothermal *t*s. [Color figure can be viewed in the online issue, which is available at wileyonlinelibrary.com.]

saturation-type dendrite; this indicated a slow nucleation followed by a comparatively fast growth.[23]

There was a big difference in the spherulite sizes under the same view of PLM, and the spherulite sizes on edge were larger than those in the center. To study the spherulite size under different isothermal *t*s, we counted the maximum spherulite sizes on edge under different isothermal *t*s, and the results are shown in Figure 13. As shown in Figure 13, the spherulite sizes of PA66-10 were smaller than those of PA66-0; this indicated that to form the same spherulite size, the molecules of PA66-10 may

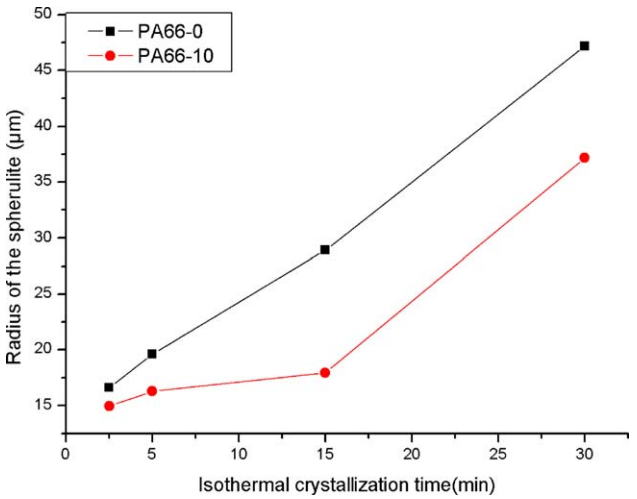

Figure 13. Plots of the isothermal *t* versus the radius of the spherulites of PA66-0 and PA66-10. [Color figure can be viewed in the online issue, which is available at wileyonlinelibrary.com.]

have needed more time than those of PA66-0. This result shows that the addition of CEPPA to the molecular chain of PA66 hindered the spherulite growth.

CONCLUSIONS

The nonisothermal crystallization kinetics of PA66-0 and PA66-10 were studied by DSC and analyzed by *n* and the Jeziorny, Mo, and Kissinger methods. The good results suggest that these methods were reasonable in the analysis of the nonisothermal crystallization of PA66-0 and PA66-10.The results show that

1. It seemed that when Φ was 15°C/min, PA66-0 formed a more perfect crystal, whereas to get a good crystallization for PA66-0, Φ was needed in the range of 10–15°C/min.
2. After CEPPA was incorporated into the main chain of PA66-0, the crystallization mechanism of PA66-0 was changed, except in the prime stage, which belonged to a stage of slow nucleation according to the result of the POM test when Φ were 15 and 20°C/min.
3. Jeziorny's and Mo's methods showed that the addition of CEPPA slowed the rate of crystallization of PA66-0. This was confirmed by the Kissinger method, which was also confirmed by the POM test. In addition, the POM test showed that the addition of CEPPA to the molecular chain of PA66 changed the spherulitic birefringence of PA66. The signs of the spherulitic birefringence of PA66 and PA66-10 were found to depend on the isothermal *t*. When the isothermal *t* value was from 2.5 to 30 min, the signs of the birefringence of PA66-0 changed in the following order:

Positive → Mixed → Weekly mixed → Positive

The signs of the birefringence of PA66-10 changed in another order:

Mixed → Positive → Mixed → Weekly mixed

ACKNOWLEDGMENTS

The authors thank the Thermal Analysis Test Laboratory at the School of Materials Science and Chemical Engineering of the Tianjin University of Science and Technology.

REFERENCES

1. Li-Sheng, W.; Hui-Bao, K.; Shu-Bo, W.; Yong, L.; Ran, W. *Fluid Phase Equilib.* **2007**, *258*, 99.
2. Haiming, L.; Rui, W.; Xi, X. *J. Appl. Polym. Sci.* **2010**, *121*, 3131.
3. Liang-Jie, L.; Rong-Tao, D.; Jun-Bo, Z.; Xiu-Li, W.; Li, C.; Yu-Zhong, W. *Ind. Eng. Chem. Res.* **2010**, *52*, 5326.
4. Jawed, A.; Chesterfield, M. U. S. Pat. 5,750,603, **1997**.
5. Sheng-Long, T.; Lian-Xin, M.; Xiao-Guang, S.; Xu-Dong, T. *High Perform. Polym.* **2014**, 1, DOI: 10.1177/0954008314539358.
6. Xiao-Ting, C.; Xu-Dong, T.; Ming-Zhu, Z. *J. Tianjin Univ. Sci. Technol.* **2004**, *19*, 7.
7. Gupta, A. K.; Rana, S. K.; Deopura, B. L. *J. Appl. Polym. Sci.* **1994**, *51*, 231.
8. Jeziorny, A. *Polymer* **1978**, *19*, 1142.
9. Herrero, C. R.; Acosta, J. L. *Polym. J.* **1994**, *26*, 786.
10. Sunil, P.; Lonkar, S.; Morlat-Therias, N.; Caperaa, F.; Leroux, J. L.; Gardette, R. P. *Polymer* **2009**, *50*, 1505.
11. Liu, T. X.; Mo, Z. S.; Wang, S.; Zhang, H. F. *Polym. Eng. Sci.* **1997**, *37*, 568.
12. Minying, L.; Qingxiang, Z.; Yudong, W.; Chenggui, Z.; Zhishen, M.; Shaokui, C. *Polymer* **2003**, *44*, 2537.
13. Liu, S. Y.; Yu, Y. N.; Cui, Y.; Zhang, H. F.; Mo, Z. S. *J. Appl. Polym. Sci.* **1998**, *70*, 2371.
14. Zhishen, M. *Chin. J. Polym. Sci.* **2008**, *7*, 657.
15. Kissinger, M. *J. Res. Natl. Stand.* **1956**, *57*, 217.
16. Defeng, W.; Chixing, Z.; Xie, F.; Dalian, M.; Bian, Z. *J. Appl. Polym. Sci.* **2006**, *99*, 3257.
17. Caze, C.; Devaux, E.; Crespy, A.; Cavrot, J. P. *Polymer* **1997**, *38*, 497.
18. Minying, L.; Qingxiang, Z.; Yudong, W.; Chenggui, Z.; Zhishen, M.; Shaokui, C. *Polymer* **2003**, *44*, 2537.
19. Caze, C.; Devaux, A.; Crespy, J.; Carrot, P. *Polymer* **1997**, *38*, 497.
20. Pramanik, N. K.; Haldar, R.; Niyogi, U. K.; Alam, S. *J. Macromol. Sci. Pure Appl. Chem.* **2014**, *51*, 296.
21. Fangyang, L.; Changlian, X.; Jianbing, Z.; Shaolong, L.; Yu-Zhong, W. *Thermochim. Acta* **2013**, *568*, 38.
22. Lanqing, Z.; Yuying, H. *China Plast.* **2008**, *22*, 33.
23. Bassett, D. C. Principles of Polymer Morphology; Cambridge University Press: Cambridge, England, **1981**.